

# Exploring Entanglement Characteristics in Disordered Free Fermion Systems through Random Bi-Partitioning

Mohammad Pouranvari\*

*Department of Solid-State Physics, Faculty of Science, University of Mazandaran, Babolsar, Iran.*

(Dated: September 26, 2023)

This study investigates the entanglement properties of disordered free fermion systems undergoing an Anderson phase transition from a delocalized to a localized phase. The entanglement entropy is employed to quantify the degree of entanglement, with the system randomly divided into two subsystems. To explore this phenomenon, one-dimensional tight-binding fermion models and Anderson models in one, two, and three dimensions are utilized. Comprehensive numerical calculations reveal that the entanglement entropy, determined using random bi-partitioning, follows a volume-law scaling in both the delocalized and localized phases, expressed as  $EE \propto L^D$ , where  $D$  represents the dimension of the system. Furthermore, the role of short and long-range correlations in the entanglement entropy and the impact of the distribution of subsystem sites are analyzed.

## I. INTRODUCTION

The study of entanglement properties has garnered significant attention among condensed matter physicists over the last decade. This is primarily due to the fact that entanglement serves as a powerful indicator of correlations within a system, rendering it a promising candidate for characterizing the phase of the system [1–6]. Various measures of entanglement have been proposed for quantifying it, with the most widely accepted being the entanglement entropy (EE). In addition to EE's utility for pure states, alternative measures for mixed states have also been introduced [2, 7–10]. EE is typically computed within a bi-partitioned system, where the system is divided into two subsystems. For instance, in a system comprising  $L$  sites, sites numbered from 1 to  $L/2$  constitute the subsystem, while the remaining sites constitute the environment. As EE indirectly quantifies correlations within the system, its calculation within a bi-partitioned system enables the measurement of both short-range correlations near the boundary of the subsystems and long-range correlations within the system. These short-range correlations are responsible for what is commonly referred to as the area-law, signifying that the amount of entanglement between two subsystems is proportional to the area of the boundary between them [11–15]. However, in systems characterized by long-range hopping amplitudes and, consequently, long-range correlations in the delocalized phase, this area law is violated. As demonstrated in our previous work, for a one-dimensional system with long-range hopping amplitudes, EE behaves in accordance with a volume law, rather than an area law [6].

We should note that the manner in which we partition the system into two subsystems profoundly impacts the information we can glean from the entanglement [16, 17]. To obtain a comprehensive understanding of the system, it is imperative to employ various partitioning schemes.

In this context, the concept of *random partitioning* has recently emerged, where the subsystems are chosen randomly [18–20]. To calculate entanglement entropy (EE) with random partitioning, the following procedure is typically employed: for a system comprising  $L$  sites, the size of the subsystem can vary from 1 up to  $L - 1$ , and the selection of sites belonging to the subsystem is done randomly (each site  $i$  has a probability  $p_i$  of belonging to the subsystem). Ultimately, an appropriate average is computed over all such selections. In the case where a constant probability is assigned, denoted as  $p_i = \text{constant}$ , EE with random partitioning at an arbitrary temperature is expressed as follows:

$$EE(T, p) = \sum_{n=1}^L \overline{EE}_n(T) \binom{L}{n} p^n (1-p)^{L-n}, \quad (1)$$

Here,  $\overline{EE}_n$  represents the disorder-averaged EE for subsystems with  $n$  sites.

In a related paper [20], we conducted an investigation into the entanglement properties of a random spin 1/2 chain at arbitrary temperature, employing a random partitioning approach. Our study unveiled that the entanglement entropy (EE) exhibits a volume-law behavior at arbitrary temperature, with a pre-factor dependent on both temperature ( $T$ ) and the partitioning probability ( $p$ ). We elucidated how EE serves as a revealing metric for the count of singlet and triplet $_{\uparrow\downarrow}$  states distributed throughout the system, each characterized by distinct bond lengths within the framework of the real-space renormalization group (RSRG) method, wherein pairs of spins are placed in singlet or triplet states. Consequently, our work demonstrated that EE, when determined through random partitioning, captures both short-range and long-range correlations across the entire system.

In this report, our focus shifts to exploring the entanglement properties of systems undergoing an Anderson phase transition between delocalized and localized states, utilizing a random bi-partitioning scheme. By "random bi-partitioning," we refer to the following procedure: the

\* m.pouranvari@umz.ac.ir

system is divided evenly into two subsystems, each comprising  $L/2$  sites, with the selection of sites for each subsystem being done randomly. Our inquiries revolve around several key aspects: What are the EE characteristics when employing this partitioning method? Does this approach to EE characterization effectively discern the Anderson phase transition, signifying distinct EE behaviors in delocalized and localized states? Finally, what insights can be gained about system correlations by manipulating the distribution of sites within the subsystems?

To address the aforementioned inquiries, we conduct exhaustive numerical computations employing one-dimensional tight-binding models exhibiting delocalized-localized phase transitions. Additionally, we employ the Anderson model in one, two, and three dimensions. Detailed descriptions of these models and our EE calculation methodology are provided in Section II. The outcomes of our investigations are presented in Section III. Finally, we draw our conclusions and outline future prospects in Section IV.

In this report, we embark on an exploration into the intriguing realm of entanglement properties using the innovative framework of random bi-partitioning. Our motivation stems from the distinctive nature of this approach, which introduces a fresh perspective on the study of entanglement dynamics amidst Anderson phase transitions. While our analysis may not conclusively distinguish between the delocalized and localized phases, it contributes a valuable dimension to the broader understanding of quantum phase transitions. By employing random bi-partitioning, we aspire to provide a nuanced perspective on the behavior of entanglement entropy (EE) and its intricate interplay with the Anderson phase transition. In doing so, we aim to uncover subtle correlations and nuanced behaviors that may not be immediately apparent using traditional partitioning methods. This paper's significance lies in its capacity to deepen our appreciation of entanglement in disordered systems and the complex interplay between quantum states and phase transitions, paving the way for further explorations and refinements in this fascinating field.

## II. MODELS AND METHOD

In this report, we investigate tight-binding fermion lattice models in one, two, and three dimensions, with a focus on their phase transitions between delocalized and localized phases. It is essential to emphasize that these models are well-established in the literature, and their properties have been extensively studied in previous research. Our primary objective is to employ these known models to explore the behavior of entanglement entropy (EE) within the framework of random bi-partitioning, a novel approach explained in the subsequent sections.

The first model under consideration is the random dimer model (RD), described by the following Hamilto-

nian:

$$H = -t \sum_{i=1}^{L-1} \left( c_i^\dagger c_{i+1} + c_{i+1}^\dagger c_i \right) + \sum_{i=1}^L \epsilon_i c_i^\dagger c_i, \quad (2)$$

where  $L$  represents the system size,  $c_j$  ( $c_j^\dagger$ ) denotes the annihilation (creation) fermion operator at site  $j$ , and open boundary conditions are employed. Here,  $t$  represents the tunneling amplitude, which we set to  $t = 1$  as our energy scale. The on-site energies  $\epsilon_i$  can take on one of two constant values,  $\phi_a$  and  $\phi_b$ . These values are randomly assigned, with a unique feature of assigning  $\phi_b$  to two successive sites, leading to its designation as the random dimer model. It has been established [21] that the state at the resonant energy  $E_{res} = \phi_b$  exhibits delocalization when  $-2t \leq \phi_a - \phi_b \leq 2t$ , while all other states are localized. For our calculations, we set  $\phi_a = 0$ , resulting in delocalized states when  $-2 \leq \phi_b \leq 2$ . Due to this symmetry, we consider only the positive range in our calculations. We set the Fermi energy as  $E_F = \phi_b$ . It is crucial to note that in this model, only one single-particle state of the system, without backscattering, displays delocalization at the resonant energy. Consequently, we do not encounter a conventional Anderson phase transition with mobility edges separating delocalized and localized states in this particular model.

The second model we investigate is the Aubry-Andre (AA) model, characterized by the same Hamiltonian form as Eq. (2). It possesses a constant hopping amplitude, denoted as  $t = 1$ , while the onsite energies exhibit incommensurate periodicity:

$$\epsilon_i = 2\lambda \cos(2\pi ib + \theta), \quad (3)$$

where  $b = (1 + \sqrt{5})/2$  represents the golden ratio, and  $\theta$  values are randomly drawn from a uniform distribution within the range  $[-\pi, \pi]$ . It is important to note that in our numerical calculations, the phase  $\theta$  remains consistent across all sites for a single realization. The behavior of all states within the system is characterized by delocalization when  $\lambda < 1$ , while localization occurs for  $\lambda > 1$ . As a result, a distinctive Anderson phase transition emerges at  $\lambda = 1$  [22, 23]. For our calculations, we set the Fermi energy as  $E_F = 0$ . It is worth mentioning that both the random dimer (RD) and Aubry-Andre (AA) models exclusively feature nearest-neighbor hopping amplitudes.

Moving forward, our attention shifts to the power-law bond-disordered Anderson model (PRBA), which is a one-dimensional model characterized by the following Hamiltonian:

$$H = \sum_{i,j=1, i \neq j}^L \frac{w_{ij}}{|i-j|^\alpha} c_i^\dagger c_j, \quad (4)$$

with zero on-site energies. The  $w$  values are random numbers uniformly distributed in the range  $[-1, 1]$ , satisfying the condition  $w_{ij} = w_{ji}$ . The states within the system

exhibit delocalization for  $\alpha < 1$ , transitioning to localization for  $\alpha > 1$  [24]. Similar to the previous models, we set the Fermi energy at  $E_F = 0$ . However, it is worth highlighting that unlike the RD and AA models, the PRBA model incorporates long-range hopping amplitudes.

We also investigate the Anderson model in one, two, and three dimensions (1D, 2D, and 3D) with a Hamiltonian analogous to Eq. (2), featuring constant nearest-neighbor hopping amplitudes ( $t = 1$ ). The on-site energies in this model are randomly distributed, following a Gaussian distribution with a mean of zero and a variance of  $w$ . It is well-established that in one and two dimensions, the system becomes localized with any infinitesimal level of disorder [25], thus obviating the presence of a delocalized-localized phase transition. However, for the 3D Anderson model, the system remains delocalized for small values of the disorder strength  $w$ , eventually transitioning to localization at a critical value, approximately  $w_c \approx 6.1$  [25–27]. For our calculations concerning the Anderson models in one, two, and three dimensions, we maintain the Fermi energy at  $E_F = 0$ .

To compute the entanglement entropy (EE), we first partition the system. In the case of a lattice model comprising  $L$  sites, conventional practice involves splitting the system at its midpoint, designating one half as subsystem  $A$  (see Fig. 1 (a)). However, in this report, we introduce a novel approach, namely, *random bi-partitioning*, where we randomly select  $L/2$  sites based on a uniform distribution to form subsystem  $A$  (see Fig. 1 (b) for a typical example of random bi-partitioning). Notably, the sites belonging to subsystem  $A$  can be either adjacent or widely separated, resulting in a subsystem composed of randomly distributed sites across the entire system. This represents a departure from the conventional practice of splitting the system at its midpoint.

To calculate the EE, we follow a practical method employing the correlation matrix [28]:

$$C_{ij} = \langle c_i^\dagger c_j \rangle, \quad (5)$$

where  $i$  and  $j$  traverse the indices of the randomly chosen subsystem. EE can then be determined based on the eigenvalues of the correlation matrix  $\{\eta\}$  using the following expression:

$$EE = - \sum_{i=1}^{L_A} [\eta_i \log \eta_i + (1 - \eta_i) \log(1 - \eta_i)], \quad (6)$$

where  $L_A = L/2$  represents the size of the subsystem.

### III. RESULTS

In this section, we present our detailed numerical calculations of entanglement entropy (EE) in a randomly bi-partitioned system. We investigate the behavior of EE in models with delocalized and localized phases, including

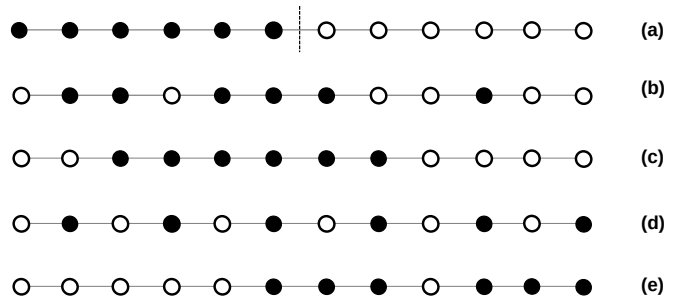


FIG. 1. Schematic representation of random bi-partitioning of the system. Sites belonging to subsystem  $A$  are colored in black, while the white sites represent the environment. In these examples, we set  $L = 12$  and  $L_A = L/2 = 6$ . (a) depicts a typical example of bi-partitioning, where 6 black sites are separated from 6 white sites by a dashed line in the middle. (b) illustrates a typical example of *random* bi-partitioning. (c) shows a limiting case where all of the subsystem sites are adjacent. (d) displays a limiting case with no adjacent sites within the subsystem. (e) demonstrates an example where the minimum number of connected sites is set to  $\ell = 3$ .

the random dimer (RD), Aubry-André (AA), and power-law bond-disordered Anderson (PRBA) models. Additionally, we explore EE in Anderson models in one, two, and three dimensions (1D, 2D, and 3D). Our primary goal is to examine the size dependence of EE and evaluate the impact of the distribution of subsystem sites on the EE in randomly bi-partitioned systems.

#### A. Random Bi-partitioning in RD, AA, and PRBA Models

First, we delve into the behavior of EE in a randomly bi-partitioned system for the RD model. The results of our numerical calculations are depicted in Fig. 2, comprising four panels.

In Panel (1), we plot EE versus  $\phi_b$  for various system sizes. Notably, a singularity emerges in the EE at the phase transition point, making it readily distinguishable. Furthermore, EE in the delocalized phase surpasses that in the localized phase.

Panel (2) showcases the plot of  $EE/L$  versus  $\phi_b$  for different system sizes. We observe that the behavior remains consistent across various sizes, with the curves overlapping in both the delocalized and localized phases.

Panel (3) presents a plot of  $EE/L$  as a function of system size. It becomes evident that  $EE/L$  converges to a fixed value for large system sizes, and this fixed value is dependent on  $\phi_b$ .

Finally, Panel (4) illustrates a log-log scale plot of EE versus system size. The resulting curve exhibits a linear trend with a slope close to 1 in both the delocalized and localized phases, indicating that  $EE$  is proportional to  $L$ ,

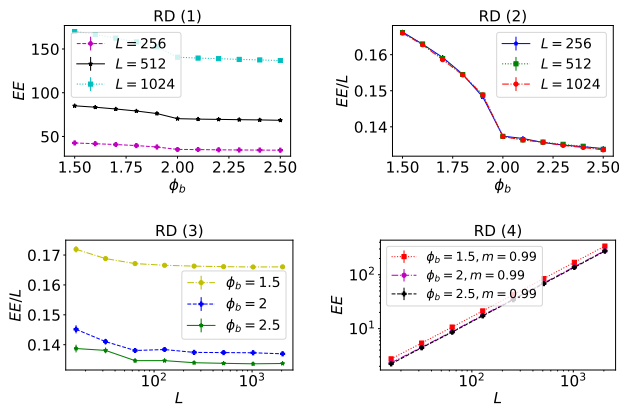


FIG. 2. Entanglement Entropy (EE) Characteristics in the Random Dimer (RD) Model with Random Bi-partitioning. **(1)** EE is depicted as a function of  $\phi_b$  for various system sizes:  $L = 256, 512, 1024$ . **(2)** The behavior of  $EE/L$  is shown for different system sizes, demonstrating a consistent trend in both delocalized and localized phases. **(3)** For system sizes exceeding approximately 100,  $EE/L$  converges to a stable value contingent upon  $\phi_b$ . **(4)** A power-law relationship between EE and system size  $L$  is evident, observed in the log-log scale where the slope, denoted as  $m$ , closely approaches 1. The Fermi energy is set to  $E_F = \phi_b$ . Each data point represents an average over  $10^4$  samples.

with the proportionality dependent solely on  $\phi_b$ . Consequently, we can express  $EE$  as  $EE = f_{RD}(\phi_b)L$  in both the delocalized and localized phases, where  $f$  represents a function solely dependent on  $\phi_b$ .

For the AA model, as shown in Fig. 4, the behavior of EE is not distinguishable at the phase transition point. Nevertheless, it is evident that EE is smaller in the localized phase compared to the delocalized phase (as seen in the 1st and 2nd plots). Based on the observations from the 3rd and 4th plots, we can conclude that  $EE = f_{AA}(\lambda)L$ , indicating a power-law behavior of EE with respect to system size in both the delocalized and localized phases.

As for the PRBA model (refer to Fig. 4), we note that EE is lower in the localized phase than in the delocalized phase. Similarly, we can conclude that  $EE = f_{PRBA}(\alpha)L$  holds true in both the delocalized and localized phases.

## B. Random Bi-partitioning in the Anderson Model in One, Two, and Three Dimensions

In this subsection, we undertake an examination of the entanglement entropy (EE) with the application of random bi-partitioning within the Anderson model across one, two, and three dimensions. It is well-established that a phase transition between delocalized and localized states exclusively manifests in the three-dimensional Anderson model, whereas all states in one and two dimensions become localized even with infinitesimal disorder

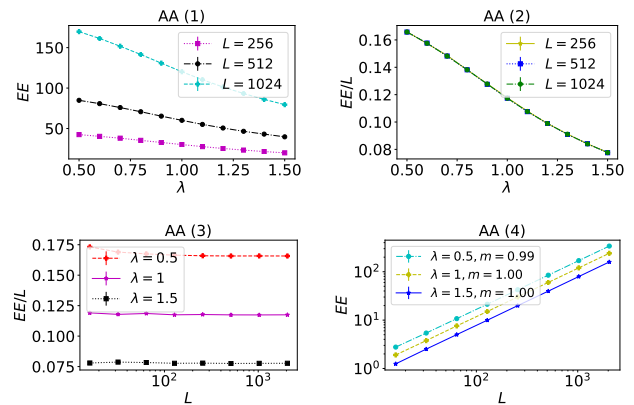


FIG. 3. Behavior of the entanglement entropy (EE) in the Aubry-Andre (AA) model under random bi-partitioning. **(1)** EE is plotted against  $\lambda$  for various system sizes  $L = 256, 512, 1024$ . **(2)** The behaviors of EE per site ( $EE/L$ ) for different system sizes consistently coincide in both delocalized and localized phases. **(3)**  $EE/L$  saturates to a constant value for system sizes beyond approximately  $\sim 100$ , depending solely on  $\lambda$ . **(4)** An observed power-law behavior of EE versus system size  $L$  (where the slope in the log-log scale, denoted as  $m$ , closely approaches 1).  $E_F$  is set to 0, and each data point results from averaging over  $10^4$  samples.

der [25]. Our numerical findings are presented in Figure 5.

The behavior of the EE in the one-dimensional (1D), two-dimensional (2D), and three-dimensional (3D) Anderson models reveals a characteristic power-law relationship. As illustrated in Figure 5, the log-log plots' slopes are consistently close to unity (1). This observation leads us to the conclusion that, in the Anderson model, the entanglement entropy ( $EE$ ) scales as  $L^D$  for both the delocalized and localized phases.

## C. Connected and Disconnected Subsystems

In the aforementioned calculations, which employed random bi-partitioning, it is crucial to note that the sites constituting the subsystem were selected at random, following a uniform distribution. Consequently, the subsystem may consist of either connected or disconnected sites, representing two distinct scenarios. These scenarios are exemplified by a subsystem composed of  $L_A$  connected sites (as depicted in Fig. 1 (c)) and a subsystem comprising  $L_A$  disconnected sites (as shown in Fig. 1 (d)).

When assessing the Entanglement Entropy (EE), we are essentially indirectly quantifying the correlations between the subsystem's sites and the remainder of the system. These correlations can exhibit either short-range or long-range behavior. Short-range correlations give rise to entanglement only when two sites belonging to different subsystems are situated in close proximity to the boundary. In contrast, long-range correlations can lead

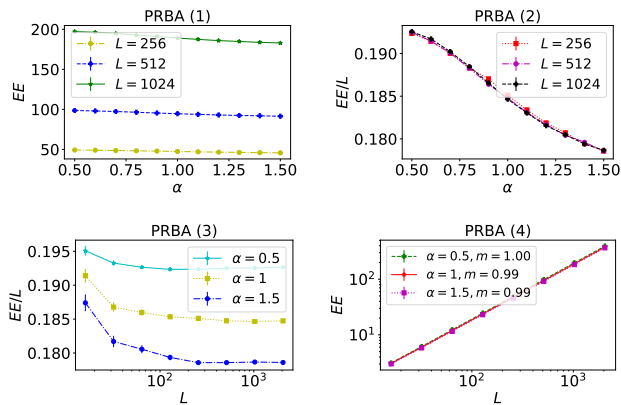


FIG. 4. Analysis of the entanglement entropy (EE) behavior in the Power-law Bond-Disordered Anderson (PRBA) model under random bi-partitioning. (1) EE is depicted as a function of  $\alpha$  for varying system sizes  $L = 256, 512, 1024$ . (2) The trends of EE per site ( $EE/L$ ) for different system sizes consistently align in both delocalized and localized phases. (3)  $EE/L$  reaches a steady state for system sizes larger than approximately  $\sim 300$ , with the steady value depending solely on  $\alpha$ . (4) A power-law relationship between EE and system size  $L$  is evident (the slope in the log-log scale, denoted as  $m$ , closely approximates 1).  $E_F$  is held constant at 0, and each data point is an average computed from  $10^4$  samples.

to entanglement even when the correlated sites are widely separated from one another.

In our investigations, the choice of subsystem composition within the random bi-partitioning method plays a pivotal role in the resulting entanglement entropy (EE). The subsystem may consist of completely disconnected sites, leading to the measurement of both short-range and long-range correlations across the entire system. Even in scenarios where the system lacks long-range correlations, a substantial EE emerges due to the inclusion of all short-range correlations. Conversely, for a fully connected subsystem, only short-range correlations in proximity to the boundary contribute to the entanglement, alongside long-range correlations.

This observation underscores the significance of the distribution of subsystem sites in EE calculations. To elucidate this point, we introduce a parameter,  $\ell$ , which represents the minimum number of connected sites within the subsystem (Fig. 1 (e) depicts the case where  $\ell = 3$ ). The value of  $\ell$  varies within the range of 1 to  $L/2$ . In Fig. 6, we present the variation of  $EE/L$  with  $\ell$  for systems of size  $L$ , considering the RD, AA, and PRBA models.

As demonstrated in Fig. 6, an increase in the parameter  $\ell$  results in a corresponding decrease in entanglement. This behavior is consistent with expectations, as a higher value of  $\ell$  diminishes the contributions to EE stemming from short-range correlations, leading to a reduction in EE.

However, the decrease in the EE is not uniform across

TABLE I. Table of the ratio of change in  $\log_{10} EE$  when increasing the minimum number of connected sites,  $\ell$ , from 1 to  $L/2 = 256$  in the delocalized phase  $\Delta_D$  and in the localized phase  $\Delta_L$ , for RD, AA, and PRBA models, as per the data in Fig. 6.

Model	$\Delta_D$	$\Delta_L$
RD	0.81	1.05
AA	0.93	1.23
PRBA	0.15	0.86

all considered models. To quantify these variations, we introduce a measure that characterizes the change in  $\log_{10} EE$  as we vary  $\ell$  from 1 to  $L/2$  in both delocalized and localized phases:

$$\Delta_{D/L} = \frac{\log_{10}[EE_{\ell=1}] - \log_{10}[EE_{\ell=L/2}]}{\log_{10}[EE_{\ell=1}]}, \quad (7)$$

where  $\Delta_D$  ( $\Delta_L$ ) represents the ratio of change in the delocalized (localized) phase. Specifically, for the delocalized phase, we set  $\phi_b = 1.5$  for the RD model,  $\lambda = 0.5$  for the AA model, and  $\alpha = 0.5$  for the PRBA model. In contrast, for the localized phase, we choose  $\phi_b = 2.5$  for the RD model,  $\lambda = 1.5$  for the AA model, and  $\alpha = 1.5$  for the PRBA model, considering parameter values deep within each respective phase. The numerical results are tabulated in Table I.

To summarize our observations, we note the following:

Firstly, we consistently observe that the decrease in the entanglement entropy (EE) is more pronounced in the localized phase compared to the delocalized phase, i.e.,  $\Delta_L > \Delta_D$ . This phenomenon can be attributed to the presence of both short and long-range correlations in the delocalized phase. In contrast, the localized phase predominantly exhibits short-range correlations. Consequently, increasing  $\ell$  in the localized phase results in the omission of a significant portion of short-range correlations, leading to a more substantial reduction in EE.

Secondly, it is worth highlighting that  $\Delta_D$  for the PRBA model is smaller than that of the RD and AA models. This difference can be attributed to the distinctive hopping amplitudes in the PRBA model. Specifically, the PRBA model features long-range hopping amplitudes, which differ from the RD and AA models that primarily involve nearest-neighbor hopping amplitudes. Consequently, the PRBA model exhibits longer-range correlations, resulting in a relatively smaller decrease in the entanglement entropy in the delocalized phase compared to the RD and AA models, which primarily rely on short-range hopping amplitudes.

These observations shed light on the intricate interplay between correlation lengths, hopping amplitudes, and the behavior of entanglement entropy in diverse phases of the studied models.

In our analysis of the entanglement entropy (EE) as a function of the system size  $L$  for various values of  $\ell$ ,

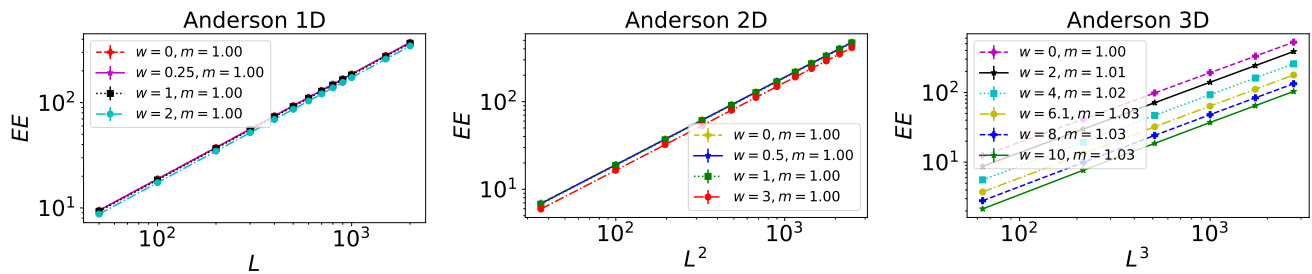


FIG. 5. Scaling behavior of the entanglement entropy ( $EE$ ) with respect to the system volume for the Anderson models in one dimension (1D), two dimensions (2D), and three dimensions (3D), depicted in the left, middle, and right panels, respectively. The log-log plots exhibit power-law scaling, with the slope ( $m$ ) of the lines consistently approximating unity (1).  $E_F$  is set to 0 for all cases, and each data point is obtained by averaging over  $10^4$  samples for the 1D model,  $10^3$  samples for the 2D model, and  $10^2$  samples for the 3D model.

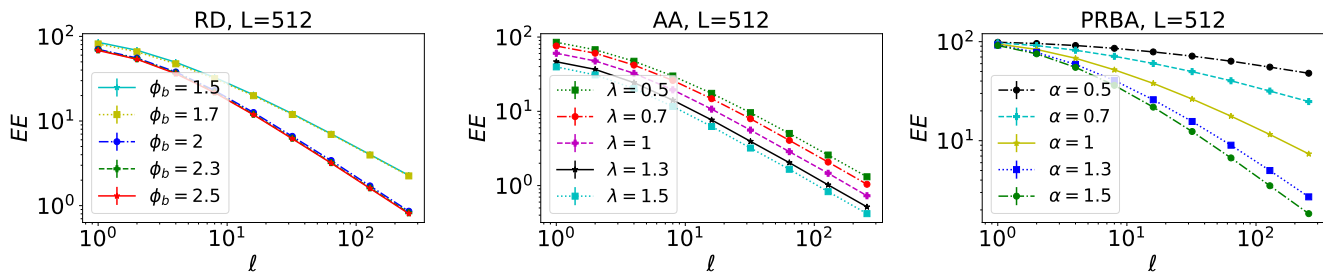


FIG. 6. Variation of the Entanglement Entropy ( $EE$ ) with the minimum number of connected sites, denoted as  $\ell$ , ranging from 1 to  $L/2 = 256$  for a system of size  $L = 512$  in the Random Disordered (RD) model (left panel), Aubrey-André (AA) model (middle panel), and Power-Law Bond-Disordered Anderson (PRBA) model (right panel). The  $EE$  exhibits a decreasing trend as  $\ell$  increases, with this decrease being more pronounced in the localized phase compared to the delocalized phase. Each data point is obtained by averaging over  $10^4$  samples (see Table I).

presented in Fig. 7, we made the following observations:

i) As expected, the  $EE$  consistently exhibits lower values in the localized phase when compared to the delocalized phase, across all considered values of  $\ell$  and system sizes.

ii) We observed a notable transition from a volume-law to an area-law scaling behavior as  $\ell$  is increased. For smaller  $\ell$  values, the  $EE$  displays rapid linear growth concerning the system size, adhering to a volume-law scaling. Conversely, as  $\ell$  is increased, the rate of  $EE$  growth diminishes, resulting in a saturation behavior that conforms to an area-law scaling.

iii) It is noteworthy that the saturation point occurs at smaller values of  $\ell$  in the localized phase compared to the delocalized phase.

iv) The PRBA model, characterized by long-range hopping amplitudes, exhibits distinct behavior. In the delocalized phase, the rate of  $EE$  increase concerning the system size is notably higher for all choices of  $\ell$  compared to the other models.

These findings provide valuable insights into the intricate scaling behaviors of  $EE$ , which depend on the phase of the system, the subsystem size, and the range of hopping amplitudes present in the model.

## IV. CONCLUSION

In this study, we have examined the entanglement properties of disordered free fermion systems by employing random bi-partitioning. The calculation of entanglement entropy ( $EE$ ) involves dividing the system into two subsystems, typically achieved by cutting the system at the middle and considering the first half as the subsystem. However, in this report, we have adopted an alternative approach by randomly selecting sites from the entire system to form the subsystem. This unconventional subsystem configuration has implications for the resulting entanglement properties.

Our analysis focused on the behavior of  $EE$  in free fermion models with delocalized and localized phases, specifically utilizing Anderson models in one, two, and three dimensions. We have found that the behavior of  $EE$  remains smooth across the phase transition point, consistent with our previous conclusions (Ref. [20]) that  $EE$  with random partitioning captures both long-range and short-range correlations throughout the system. Consequently, as we traverse the phase transition from the delocalized phase to the localized phase, the long-range correlations decrease, but short-range correlations persist



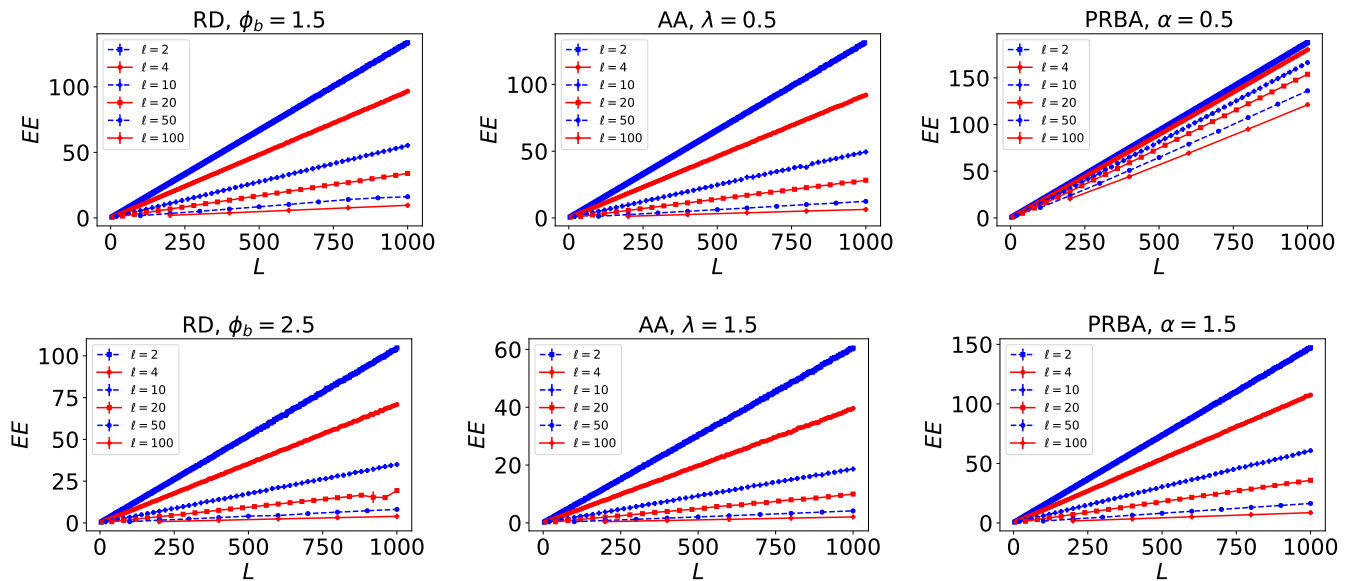


FIG. 7. Entanglement entropy (EE) versus system size  $L$  is shown in the top panels for the delocalized phase and in the bottom panels for the localized phase. The plots depict the behavior of the RD model (left panels), AA model (middle panels), and PRBA model (right panel). An increase in the parameter  $\ell$  leads to a crossover from a volume-law to an area-law scaling. Each data point represents the average over  $10^4$  samples.

throughout the system.

Furthermore, we have observed that EE increases with increasing system size, exhibiting a power-law scaling with system size ( $L$ ) in  $D$  dimensions:  $EE \propto L^D$  in both the delocalized and localized phases. These findings are based on detailed numerical calculations performed on free fermion models, including Anderson models in one, two, and three dimensions.

Additionally, we have examined the influence of subsystem site distribution on EE and noted that having more adjacent sites belonging to the subsystem leads to a decrease in EE. This observation can be attributed to the indirect measurement of correlations by EE, encompassing both short-range and long-range correlations. Increasing the number of connected sites in the subsystem results in the loss of information regarding short-range correlations. Moreover, in the delocalized phase, when significant long-distance hopping amplitudes exist in the Hamiltonian, EE demonstrates greater robustness to changes in site distribution.

It is worth mentioning that the aforementioned random partitioning can also be applied to the partitioning in momentum space (Ref. [29]), where the distribution

of subsystem sites directly impacts occupied and unoccupied levels.

In conclusion, this study represents one of the initial investigations into the entanglement properties of disordered free fermion systems exhibiting delocalized-localized phase transitions. As such, it contributes to the growing body of research exploring the behavior of entanglement entropy in these systems. The use of random bi-partitioning provides a unique approach to examining the interplay between subsystem configurations, phase transitions, system dimensions, and correlation effects. These findings hold significance for the physics community, shedding light on the intricate nature of entanglement in disordered fermion systems and their transition between delocalized and localized phases.

## ACKNOWLEDGMENTS

The author gratefully acknowledge the high performance computing center of university of Mazandaran for providing computing resource and time.

- 
- [1] K. Le Hur, P. Doucet-Beaupré, and W. Hofstetter, Phys. Rev. Lett. **99**, 126801 (2007).
  - [2] R. Horodecki, P. Horodecki, M. Horodecki, and K. Horodecki, Rev. Mod. Phys. **81**, 865 (2009).
  - [3] N. Laflorencie, Physics Reports **646**, 1 (2016).
  - [4] G. Vidal, J. I. Latorre, E. Rico, and A. Kitaev, Phys. Rev. Lett. **90**, 227902 (2003).
  - [5] P. W. Anderson, Phys. Rev. **109**, 1492 (1958).
  - [6] M. Pouranvari and K. Yang, Phys. Rev. B **89**, 115104 (2014).
  - [7] S. Szalay, Phys. Rev. A **92**, 042329 (2015).

- [8] V. Vedral, M. B. Plenio, M. A. Rippin, and P. L. Knight, *Phys. Rev. Lett.* **78**, 2275 (1997).
- [9] V. Alba, M. Fagotti, and P. Calabrese, *Journal of Statistical Mechanics: Theory and Experiment* **2009**, P10020 (2009).
- [10] T.-C. Lu and T. Grover, *ArXiv e-prints* (2018), arXiv:1808.04381 [cond-mat.stat-mech].
- [11] J. Eisert, M. Cramer, and M. B. Plenio, *Rev. Mod. Phys.* **82**, 277 (2010).
- [12] M. M. Wolf, *Phys. Rev. Lett.* **96**, 010404 (2006).
- [13] G. Vitagliano, A. Riera, and J. I. Latorre, *New Journal of Physics* **12**, 113049 (2010).
- [14] T. Koffel, M. Lewenstein, and L. Tagliacozzo, *Phys. Rev. Lett.* **109**, 267203 (2012).
- [15] B. Swingle, *Phys. Rev. Lett.* **105**, 050502 (2010).
- [16] Z. Moradi and J. Abouie, *Journal of Statistical Mechanics: Theory and Experiment* **2016**, 113101 (2016).
- [17] N. Ahmadi, J. Abouie, and D. Baeriswyl, *Phys. Rev. B* **101**, 195117 (2020).
- [18] S. Vijay and L. Fu, *Phys. Rev. B* **91**, 220101 (2015).
- [19] G. Roósz, I. A. Kovács, and F. Iglói, *The European Physical Journal B* **93**, 8 (2020).
- [20] M. Pouranvari, *Physica A: Statistical Mechanics and its Applications* **624**, 128908 (2023).
- [21] D. H. Dunlap, H.-L. Wu, and P. W. Phillips, *Phys. Rev. Lett.* **65**, 88 (1990).
- [22] S. Aubry and G. André, *Ann. Israel Phys. Soc* **3**, 18 (1980).
- [23] S. Ganesan, J. H. Pixley, and S. Das Sarma, *Phys. Rev. Lett.* **114**, 146601 (2015).
- [24] R. P. A. Lima, H. R. da Cruz, J. C. Cressoni, and M. L. Lyra, *Phys. Rev. B* **69**, 165117 (2004).
- [25] P. Markos, *arXiv preprint cond-mat/0609580* (2006).
- [26] K. Slevin and T. Ohtsuki, *Journal of the Physical Society of Japan* **87**, 094703 (2018), <https://doi.org/10.7566/JPSJ.87.094703>.
- [27] K. Slevin and T. Ohtsuki, *New Journal of Physics* **16**, 015012 (2014).
- [28] I. Peschel, *Journal of Physics A: Mathematical and General* **36**, L205 (2003).
- [29] I. Mondragon-Shem, M. Khan, and T. L. Hughes, *Phys. Rev. Lett.* **110**, 046806 (2013).